Influence of x-ray beam spatial coherence on the diffuse scattering from multilayer mirrors

V. A. Chernov
Institute of Catalysis, Novosibirsk, Russia and Siberian Synchrotron Radiation Center, Budker Institute of Nuclear Physics, 11 Lavrentiev Prospect, Novosibirsk, Russia

V. I. Kondratiev
Siberian Synchrotron Radiation Center, Budker Institute of Nuclear Physics, 11 Lavrentiev Prospect, Novosibirsk, Russia

N. V. Kovalenko
Budker Institute of Nuclear Physics, 11 Lavrentiev Prospect, Novosibirsk, Russia

S. V. Mytnichenko[a] and K. V. Zolotarev
Institute of Solid State Chemistry, Novosibirsk, Russia and Siberian Synchrotron Radiation Center, Budker Institute of Nuclear Physics, 11 Lavrentiev Prospect, Novosibirsk, Russia

(Received 2 April 2002; accepted 10 September 2002)

The improved spatial coherence of a synchrotron radiation beam was shown experimentally to stimulate additional diffuse scattering of x rays diffracted from x-ray multilayer mirrors. Although the large-scale (tens of microns) roughness does not affect Bragg diffraction from multilayers, its presence causes phase shifts at the wave packet front. This leads to partial decay of the coherent wave packet and creates additional diffuse scattering. Additional scattering from this mechanism was observed at angles of incidence corresponding to the Bragg and Kiessig maximum angles. The properties of this scattering caused by large-scale roughness, observed due to improved x-ray beam spatial coherence, were shown experimentally to be different from those of diffuse scattering previously reported when the incoming or outgoing angle is equal to the Bragg angle. Typical breaks in the diffuse scattering intensity due to the standing-wave effect are absent, and there is obvious asymmetry of the diffuse scattering cross section around the incoming and outgoing angles. Due to the small angle of incidence, the coherently irradiated area has very different dimensions parallel and perpendicular to the beam, which leads to the observed scattering being concentrated in the specular diffraction plane defined by the incident and reflected wave vectors. © *2002 American Institute of Physics.* [DOI: 10.1063/1.1518131]

I. INTRODUCTION

Diffuse scattering, which inevitably accompanies specular reflection, is an undesirable phenomenon that hampers the development of x-ray multilayer optics. On the other hand, x-ray diffuse scattering measurements provide a useful tool for surface and interfacial roughness studies that has aroused much interest in the last decade. A brief survey of scientific progress in x-ray diffuse scattering from multilayers starts with Refs. 1 and 2 in which the replication of rough multilayer interfaces was shown to cause resonant amplification of diffuse scattering resulting in the observation of a ''quasi-Bragg sheet'' of diffuse scattering. The earliest experimental observations of quasi-Bragg diffuse scattering were seen by several groups.[3–6] Special features arise in the diffuse scattering intensity when the incoming or outgoing angle is nearly equal to the Bragg angle. When the first case (incoming angle nearly equal to the Bragg angle) was studied experimentally,[7] the features observed in the diffuse scattering intensity were explained by the location of the standing wave that appeared as a result of interference of the incident and specularly reflected fields. Diffuse scattering features for the outgoing angle equal to the Bragg angle were observed independently by two groups.[4,5] A theoretical explanation of these phenomenona was found by extending the distorted wave Born approximation (DWBA), previously used to calculate diffuse scattering from single surfaces,[8] to the case of multilayers.[9] Finally, it is necessary to cite works[7,10,11] where the diffuse scattering was studied as a function of the momentum transfer normal to the specular diffraction plane.

We think, however, that much work is still required on the diffuse scattering technique both from the point of view of theory and of experiment. One of the reasons is that diffuse scattering experiments are usually carried out at experimental facilities that were designed for conventional specular measurements. But what is sufficient for usual specular measurements proves to be inadequate for a diffuse scattering study of x-ray multilayer mirrors (XMMs). In this work we focus on an important aspect of the experimental measurements, namely, the spatial coherence of the incident x-ray beam. Progress in synchrotron radiation (SR) source development has led to continual improvement of the x-ray beam spatial coherence which, in turn, has increased the requirements on the XMM quality, making this problem highly relevant.

[a]Electronic mail: s.v.mytnichenko@inp.nsk.su

 © 2002 American Institute of Physics

Downloaded 15 May 2003 to 148.6.178.88. Redistribution subject to AIP license or copyright, see http://ojps.aip.org/japo/japcr.jsp

Roughness in XMMs may vary over a wide range of length scales from the atomic ($\sim 10^{-10}$ m) up to the macroscopic ($\sim 10^{-3}$ m). The reasons for the appearance of the interfacial roughness are also varied. At the microscopic scale (10^{-10}–10^{-7} m) the roughness mainly appears as a result of the chemical and physical processes which take place during the XMM deposition. On shorter length scales reproduction of the roughness at successive interfaces is imperfect. But the contribution of roughness on this length scale to the diffuse scattering cross section is very small, at least in the case of XMMs.

On a macroscopic scale (10^{-7}–10^{-3} m) roughness at the interfaces is well replicated from one layer to another and is mainly determined by the roughness of the substrate surface. At the micron and shorter length scales, modern substrate preparation technology for XMMs is able to produce a surface quality that is practically ideal. But unfortunately this is not the case at longer length scales. Moreover, at these scales conventional methods of XMM quality control using x-ray tubes are simply unable to detect imperfections.

When crystals are used as monochromators the degree of monochromatization ($\Delta\lambda/\lambda$) is usually about $\sim 10^{-4}$. For the wavelength $\lambda = 0.154$ nm (Cu $K\alpha$ line) this corresponds to a longitudinal coherence length of $L_{\parallel} \sim \lambda^2/\Delta\lambda \sim 1$ μm. Another important diffraction parameter is the average track length of the x-ray photon on Bragg diffraction from the XMM, $L_\tau \approx 2\tau/\theta_B$, where τ is the extinction depth. For typical XMMs the value of L_τ is of about 1 μm. Roughness on a scale longer than this will not affect Bragg diffraction from the XMM.

No specular reflection is possible unless there is an ideal surface at the micron and shorter length scales. For this range literature values of the root mean square (rms) roughness are of the order of a few tenths of a nm for typical XMMs. The requirements on XMM quality at longer length scales are not so stringent.

Nevertheless, because the transverse coherence length is given by

$$L_\perp \sim \lambda D/2s,$$

where D is the source-sample distance and s is the source size, the fact that the roughness is on a length scale longer than $L_{\parallel}$ and L_τ does not mean that diffraction from this roughness will be absent. Indeed, the diffraction pattern from this roughness will be observable due to distortion of the coherent wave packet front (Fig. 1). This phenomenon is similar to the well-known observation of a diffuse halo (speckle structure) when a coherent laser beam penetrates through a nonuniform medium.The importance of transverse coherence increases for the component which lies in the specular diffraction plane. This is due to the fact that in this case the small value of the incident angle (θ_0) will cause the coherently irradiated sample area to increase as θ_0^{-1} in the corresponding direction (Fig. 1). Note that in contrast to the values of $L_{\parallel}$ and L_τ, transverse coherence can vary over a very wide range depending on the experimental setup. Its value can amount to tens of microns when a modern SR source is used.

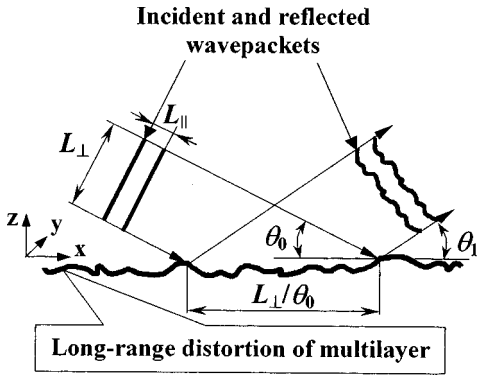

FIG. 1. Origin of the additional diffuse scattering arising as a result of distortion of the coherent wave packet front caused by macroroughness. The nature of such diffraction is quite usual. The term ''distortion of the coherent wave packet front'' was used to emphasize that the transverse coherence component considerably exceeds the longitudinal component. Clearly demonstrated is the anisotropy of the coherently irradiated XMM area. Due to the small value of the incident angle the size of this area in the direction lying in the specular diffraction plane increases as $L_\perp/\theta_0$ and can considerably exceed its size in the perpendicular direction.

It is usual to use the following form of roughness correlation function to model the x-ray diffuse scattering data:[8]

$$C(r) = \sigma^2 \exp[-(r/\xi)^{2h}],$$

where σ is the rms roughness, h is a coefficient connected with the fractal dimension $D = 3 - h$ and ξ is an effective cut-off length for the self-affine roughness induced for many physical reasons, including beam coherence. There is some discrepancy in the literature concerning the interpretation of ξ. Some authors consider ξ as the characteristic roughness length. At the same time other authors point out the importance of incident beam coherence.

In the XMM case this discrepancy may be overcome in the following manner. It is reasonable to introduce a critical value L_c so that at length scales shorter than L_c/θ_0 the XMM interfaces are practically ideal and $C(r)$ can describe their roughness. Thus, if $L_\perp$ is smaller than L_c, the value of $L_\perp$ is not so important and ξ reflects a real property of the roughness. Otherwise ($L_\perp > L_c$) ξ instead reflects the value of $L_\perp$. In this case radical modifications to the diffuse scattering will be caused by roughness at the longest length scales ($> L_c/\theta_0$). Moreover, the true specular reflection suffers ''mosaic-like'' spreading.

Numerical modeling of diffuse scattering due to distortion of the coherent wave packet front is beyond the scope of this work. Nevertheless, proceeding from the general physical criteria it is possible to make a few remarks concerning the character of the scattering from long-range roughness.

(1) The cross section of this scattering is directly proportional to the specular reflectivity coefficient of the XMM at the corresponding angle of incidence. Thus, the scattering discussed is closely associated with the diffuse scattering features at $\theta_0 = \theta_B$ (θ_B is the Bragg angle) previously observed by Kortright and co-worker[5,7] and by Savage *et al.*[4]
(2) The long length scale of the roughness does not mean that the diffraction angles will be small since it is not the

Downloaded 15 May 2003 to 148.6.178.88. Redistribution subject to AIP license or copyright, see http://ojps.aip.org/japo/japcr.jsp

size of the region of roughness itself but the size of its projection onto the wave packet front that is important:

$$\Delta\theta_1 \sim \lambda / L\theta_0,$$

where $\Delta\theta_1$ is the deviation of the outgoing angle θ_1 from the specular value and L is the length of a typical roughness feature. Since, as discussed above, in the spatial range $\leqslant \sim 1\ \mu$m the XMM surface and interfaces are ideal, the diffuse scattering discussed must be in a restricted range of angles. So at $\theta_0 \sim 3°$ and $\lambda = 0.154$ nm the angles of scattering $\Delta\theta_1 \leqslant \pm 0.2°$.

(3) Because of the small value of the incident angle the size of the coherently irradiated XMM area in the direction of the specular diffraction plane increases as $L_\perp / \theta_0$ and significantly exceeds its size in the perpendicular direction even if the transverse coherence components in both directions are comparable. This leads to the diffuse scattering discussed being concentrated in the specular diffraction plane.

(4) Since the length scale of long range roughness exceeds the value of L_τ this type of scattering excludes the typical intensity dependence on the standing wave phase under the dynamical diffraction conditions. The role of Bragg diffraction is very simple: this type of scattering is presented when the incident beam is efficiently reflected and otherwise it is absent.

This article presents experimental data for x-ray diffuse scattering from a W/Si XMM that depends on the spatial coherence of the incident beam.

II. EXPERIMENT

The W/Si XMM was deposited by magnetron sputtering onto a flat fused silica substrate. The substrate was prepared by nanodiamond polishing[12] followed by ion beam[13] polishing. It should be emphasized that the surface of the substrate used here is of the highest quality. The rms roughness was 0.3–0.4 nm according to x-ray reflectivity data and the flatness was 250 nm/2 cm (i.e., $\sim 10^{-5}$) according to interferometry data. However, we studied the surface of a typical substrate using atomic force microscopy (AFM). The data obtained are shown in Fig. 2 and one can clearly see the presence of ''roughness waves'' with amplitude of ~ 1 nm and period of $d \sim 30\ \mu$m.

The number of bilayers forming the XMM was 200. A least-squares fitting of the x-ray reflectivity data ($\lambda = 0.154$ nm) was performed to calculate the XMM optical parameters using Parrat's recursive dynamical method.[14] The XMM period was 1.47 nm ($\theta_B \sim 3°$), $\beta \approx 0.5$ and $\sigma \approx 0.6$ nm. This last value reflects both the roughness and the presence of mixed layers.

X-ray diffuse scattering measurements were performed using SR from the VEPP-3 storage ring at a wavelength $\lambda = 0.154$ nm. A channel-cut Si(111) crystal was used as the monochromator ($\Delta\lambda/\lambda \approx 2 \times 10^{-4}$) in all cases. A scintillation detector based on an FEU-130 photomultiplier with a NaI(Tl) scintillator was used. Other experimental details will be described as appropriate below.

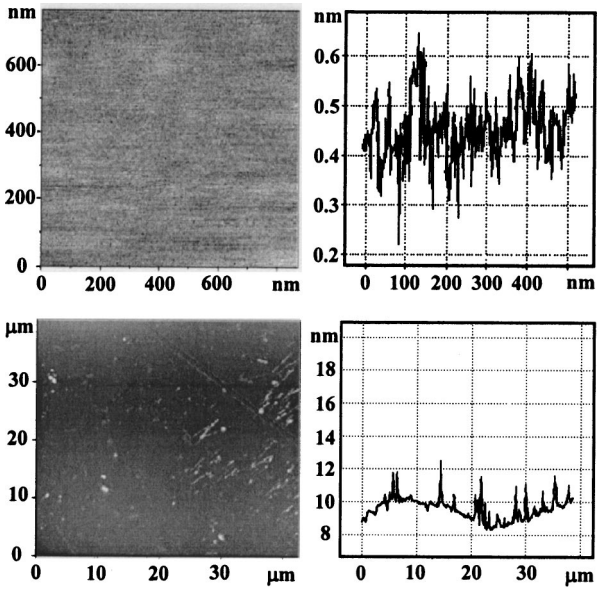

FIG. 2. AFM surface pictures of the fused silica substrate at the submicron (upper) and tens of micron (lower) spatial scales. The upper picture above demonstrates a high substrate quality with a roughness dispersion of ~0.1 nm at the submicron scale. This is not the case at the tens of microns spatial scale. Roughness waves with amplitude of ~1 nm and period of ~30 μm are easily observed. (The spikes in the lower picture are an artifact caused by dust particles on the sample surface.)

III. RESULTS AND DISCUSSIONS

The diffraction maps of the first Bragg reflection from the W/Si XMM are shown in Fig. 3. The measurements were performed in the vertical plane so that the crystal monochromator, XMM and the secondary crystal collimator Ge(111) were placed in (+,+,+) geometry. The vertical angular resolution was determined by a crystal collimator (~15–18 in.). The vertical component of the transverse coherence was estimated to have a value of about 5 μm. The maps represent sets of transverse scans (ω scans). $\theta_0 - \theta_1 \approx q_x / k\theta_B$, where q_x is the in-plane projection of the momentum transfer and k is the wave vector, is plotted parallel to the x axis and the total angle of diffraction ($\theta_0 + \theta_1 \approx q_z / k$) is parallel to the vertical axis. The q ranges of the upper map are $-3.7 \times 10^{-3}\ \text{nm}^{-1} < q_x < +3.7 \times 10^{-3}\ \text{nm}^{-1}$ and $4.13\ \text{nm}^{-1} < q_z < 4.42\ \text{nm}^{-1}$. Specular scans correspond to the vertical lines at $\theta_0 - \theta_1 = 0$.

For the upper map in Fig. 3 angular resolution of ~0.05° in the azimuthal direction was provided by a set of slits and the diffuse scattering signal was integrated over q_y in the range of $-2 \times 10^{-2}\ \text{nm}^{-1} < q_y < +2 \times 10^{-2}\ \text{nm}^{-1}$. In the case of the lower map in Fig. 3 a knife was inserted to block scattering in the specular diffraction plane ($q_y = 0$) and the corresponding integration range was reduced to $+1 \times 10^{-2}\ \text{nm}^{-1} < q_y < +2 \times 10^{-2}\ \text{nm}^{-1}$. The dynamical ranges of the measurements were different for these maps: $\sim 10^5 - 10^6$ for the upper map and $\sim 10^3 - 10^4$ for the lower.

The horizontal streaks in Fig. 3 are the quasi-Bragg scattering due to the coherent replication of roughness from one layer to another.[2] Note that because of the experimental geometry, the vertical streak in the lower map is not the true specular scattering. This ''quasispecular'' diffuse scattering

Downloaded 15 May 2003 to 148.6.178.88. Redistribution subject to AIP license or copyright, see http://ojps.aip.org/japo/japcr.jsp

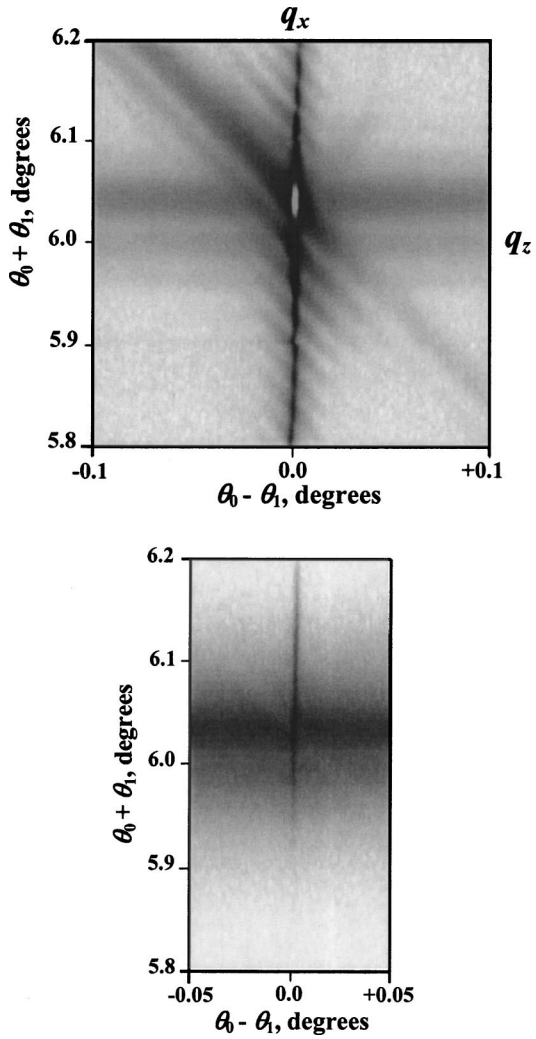

FIG. 3. Diffraction maps of scattering from a W/Si XMM near the first Bragg reflection obtained using a three-crystal diffractometer. The intensity is shown on a logarithmic scale. The main distinction in the experimental setup of these maps was that in the case of the lower map the diffuse scattering signal close to the specular diffraction plane was excluded by the use of an additional shield.

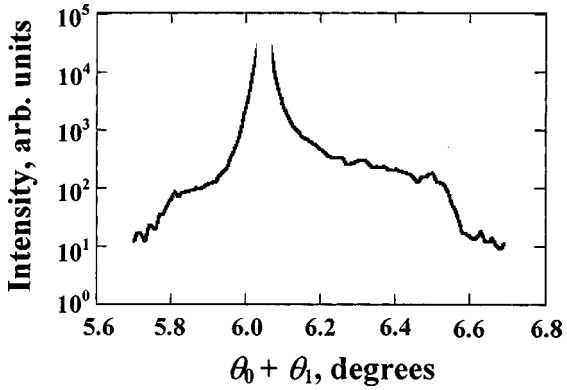

FIG. 4. Intensity distribution of the diffuse scattering along the inclined streak corresponding to $\theta_0 = \theta_B$ in the upper map of Fig. 3.

is another dynamical effect in the diffraction from the rough XMM. Mention of this effect can be found in Ref. 15. The diffuse scattering under discussion is seen as inclined streaks. This scattering is most strongly pronounced at incident angles near the Bragg angle. The rest of the inclined streaks are due to Kiessig modulations. The absence of inclined streaks in the lower map demonstrates well that the diffuse scattering discussed is concentrated in the specular diffraction plane.

It is very interesting to compare our data with those obtained from a W/C XMM by Kortright.[5] As mentioned above, the diffuse scattering discussed here and that observed in Ref. 5 are closely associated. They are described by the same term $\sim R_0 T_1$ in the DWBA[9] and have an entirely dynamical nature. Nevertheless, within the context of this article the situation realized in Ref. 5 is opposite to our situation. The reported high value of the incident beam angular spread ($\sim 0.125°$) leads to a low value of beam spatial coherence. Thus, it is reasonable to expect that the contribution of short-range (<1 μm) roughness dominates in this case as opposed to in our case. As a result the diffuse scattering features observed in Ref. 5 show evidence of standing-wave effects as breaks in the diffuse scattering intensity. In our data this effect only becomes apparent as an inclined light streak in the case of the lower map in Fig. 3 where the diffuse scattering discussed provided by the long-range (>1 μm) roughness was suppressed. In the upper map the contribution of macroscopic-scale roughness dominates and this effect is not visible.

It is necessary to point out the evident asymmetry of our data in the intensity of the "incoming" ($\theta_0 = \theta_B$) and "outgoing" ($\theta_1 = \theta_B$) streaks. In our case the incoming streak is absolutely dominant, in contrast to in Ref. 5, where these features have approximately equal intensities. This difference is not accidental and can be qualitatively explained using basic physical principles. The symmetry of the diffuse scattering cross section relative to exchanging the incoming and outgoing angles ($\theta_0 \leftrightarrow \theta_1$) is known as the reciprocity theorem[8] and is an indispensable exclusive attribute of the Born (including DWBA) approximation. The forced conservation of the incident wave energy and violation of the optical theorem by the Born approximation provide this symmetry. Thus, when energy dissipation through the incoherent diffuse scattering channel can be neglected, the diffuse scattering data should reveal the symmetry discussed (photoabsorption as another important channel is omitted in this discussion). This situation was realized in Ref. 5. The long-range roughness essentially increases the diffuse scattering cross section (the incoherent diffuse scattering channel is dominant in our case) and, consequently, causes breakdown of the Born approximation.[16] Finally, the weak presence of the outgoing streak in Fig. 3 can be explained by the higher dynamic range of the measurements of Ref. 5.

Figure 4 shows the intensity distribution along the main inclined streak of the discussed diffuse scattering in the upper map of Fig. 3. The angular range of the diffuse scattering is in rather good agreement with the above estimate. At present we are unable to give a complete explanation of the origin of the distinct asymmetry of the intensity distribution. Nevertheless, it is interesting to note that in the case of the Kiessig streaks the diffuse intensity is symmetric with respect to the specular reflection. This fact allows one to con-

Downloaded 15 May 2003 to 148.6.178.88. Redistribution subject to AIP license or copyright, see http://ojps.aip.org/japo/japcr.jsp

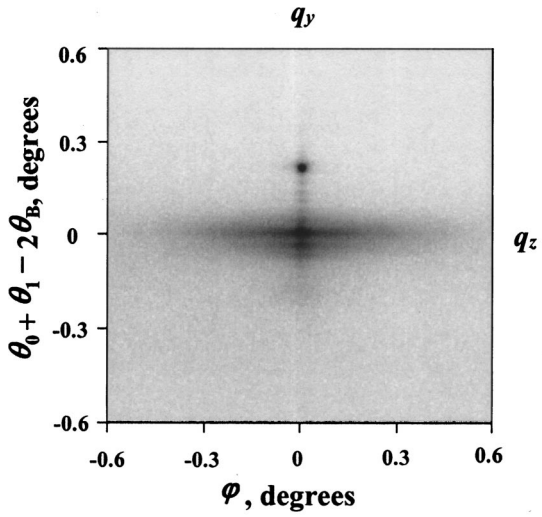

FIG. 5. Map of the scattering near the first Bragg reflection from a W/Si XMM for incident angle exceeding the Bragg angle by a value of 0.1°. The map was obtained using an image plate. The horizontal axis is the azimuthal angle, $\varphi \approx q_y/k$, and the vertical axis is the deviation of the total scattering angle ($\theta_0+\theta_1 \approx q_z/k$) from $2\theta_B$. The intensity is shown on a logarithmic scale. The dynamical range of the measurements was of about 10^4. The extended horizontal streak in the center is quasi-Bragg scattering. The upper spot is the specular reflection located at the intersection of two streaks: the horizontal streak is the quasispecular scattering and the vertical streak is the diffuse scattering discussed.

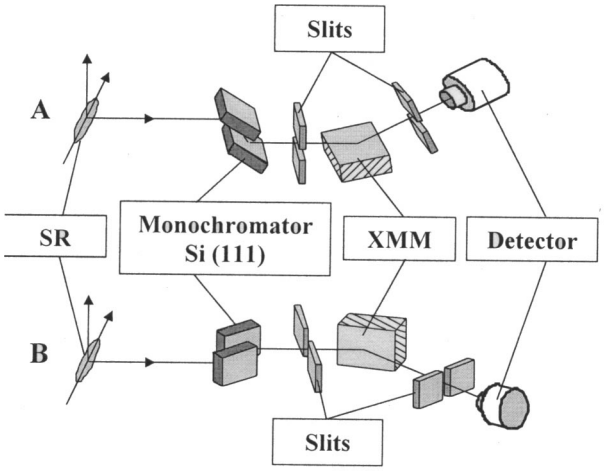

FIG. 6. Experimental setup (a) in the normal vertical geometry (source size about 250 μm, transverse coherence value about 5 μm) and (b) in the horizontal geometry (source size about 3 mm, transverse coherence value about 5 μm). In (b) the diffuse scattering due to coherent wave packet front distortion must be either absent or substantially suppressed, and this is what is observed in Fig. 7.

clude that the asymmetry discussed is caused by wave extinction under dynamical Bragg diffraction from the XMM.

Another type of map obtained using an image plate is shown in Fig. 5. The secondary crystal collimator was not used in this case. The angular resolution in the azimuthal direction of about 0.02° was provided by a set of primary collimators (100×100 μm^2) placed in front of the XMM. The vertical component of the transverse coherence was estimated to be the same as in the previous case. The horizontal axis in Fig. 5 is the azimuthal angle ($\varphi \approx q_y/k$), and the vertical axis is the deviation of the total scattering angle ($\theta_0+\theta_1 \approx q_z/k$) from $2\theta_B$. The q_y range in Fig. 5 is $-0.43\,nm^{-1} < q_y < 0.43\,nm^{-1}$. The diffuse scattering discussed is presented in Fig. 5 as the Kiessig modulated vertical streak. Note that Kiessig modulations of the scattering were not observed in the case of $\theta_0=\theta_B$ (Fig. 4). Obviously, their absence in Fig. 4 is caused by wave extinction due to dynamical diffraction. Finally, the data in Fig. 5 allow one to conclude that the inclined streaks of diffuse scattering present in Fig. 3 are not an experimental artifact caused by the use of the secondary crystal collimator.

It is possible that the scattering discussed was observed more than once in the literature. In Refs. 10 and 11 the azimuthal dependence of the diffuse scattering from a W/Si multilayer was studied and a ''hump'' near the specular diffraction plane was observed. This feature was explained as a cross-correlation effect. At the same time the authors carefully stated that this explanation has a preliminary character. Another example is the small-angle diffuse scattering study of an AlAs/GaAs superlattice[17] where intense diagonal steaks in the q_x-q_z diagram corresponding to the incident Bragg angles were observed. These features were explained as an experimental artifact connected with the use of a position-sensitive detector. We also observed similar inclined diffuse streaks in the study of a Ni/C XMM.[18] The unexpected features in the diffuse scattering disappeared during low-temperature annealing that was accompanied by a mosaic-like widening of the specular reflection.

Although the above experimental data are in good agreement with the suggestions made, more direct proof of the suggested nature of the observed diffuse scattering would be the dependence of the scattering intensity on the magnitude of transverse coherence. Assuming the undulating character of the long-range roughness, an estimation of the critical value of transverse coherence can be obtained by

$$L_c \approx d\theta_0/4,$$

and at $\theta_0 \sim 3°$, $\lambda = 0.154$ nm and $d \sim 30\,\mu$m, the value of $L_c \sim 0.5\,\mu$m.

The spatial characteristics of the VEPP-3 SR source allowed us to perform such experiments. The vertical size (perpendicular to the orbit plane) of the electron bunch is about 250 μm and the horizontal size is about 3 mm. Thus by measuring the diffuse scattering in the horizontal plane (Fig. 6) it is possible to considerably worsen the transverse coherence of the incident beam. In the experiment the source–sample distance was about 16 m and the entrance slits (100 μm) were placed in immediate proximity to the sample. The transverse coherence values were about 5 and 0.4 μm in Figs. 6(a) and (b), respectively. The secondary slits (100 μm) were placed 0.4 m from the sample. The total angular resolution of the measurements was about 0.01° [Fig. 6(a)] and 0.015° [Fig. 6(b)]. The main goal of the experiment was to perform comparative measurements of the specular and diffuse scattering intensities.

The experimental data (Fig. 7) demonstrate the difference in diffuse scattering behavior between the vertical and horizontal measurement geometries (Fig. 6). As can be seen

Downloaded 15 May 2003 to 148.6.178.88. Redistribution subject to AIP license or copyright, see http://ojps.aip.org/japo/japcr.jsp

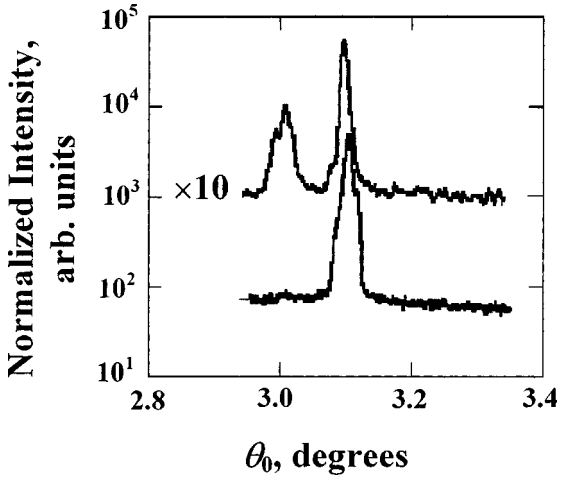

FIG. 7. Normalized intensity of diffuse scattering as a function of the incident angle θ_0 at fixed total diffraction angles (ω scans, $\theta_0+\theta_1=2\theta_B+0.2°$) in the vertical (a) (upper curve) and horizontal (b) (lower curve) geometries. The peaks at $\theta_0\approx 3.1°$ are the specular reflections, the peaks on the left at $\theta_0\approx 3.0°$ are the diffuse scattering discussed. The strong suppression of this peak in (b) is in good agreement with the suggestions made.

in Fig. 7(b) (low spatial coherence) the diffuse scattering discussed in this article is strongly suppressed which is in good agreement with the above suggestions.

IV. SUMMARY

The experimental data obtained allowed us to make the following conclusions.

(1) At a sufficiently high degree of transverse coherence of the x-ray incident beam, macroroughness with characteristic length of the order of tens of microns may cause additional diffuse scattering. This scattering is all concentrated in the specular diffraction plane and has the strongest intensity at the incident angle equal to the Bragg angle.
(2) Rapid progress in SR source development makes improvement of the XMM quality in the spatial range under discussion highly relevant.
(3) SR studies of XMM microroughness necessitate the use of unusual experimental diffuse scattering geometries that allow one to avoid measurements of diffuse scattering in the specular diffraction plane.

ACKNOWLEDGMENTS

The authors thank A. N. Artyushin, N. I. Chkhalo, I. B. Khriplovich, G. N. Kulipanov, A. V. Latushev, V. F. Pindyurin and W. Schwarzacher for their help and for useful discussions. This study was supported by the Russian Foundation for Basic Research, Grant Nos. 99-02-16671 and 00-02-17624.

[1] A. V. Andreev, A. G. Michette, and A. Renwick, J. Mod. Opt. **35**, 1667 (1988).
[2] D. G. Stearns, J. Appl. Phys. **71**, 4286 (1992).
[3] A. Bruson, C. Dufour, B. George, M. Vergant, G. Marchai, and Ph. Mangin, Solid State Commun. **71**, 1045 (1989).
[4] D. E. Savage, J. Kleiner, N. Schimke, Y.-H. Phang, T. Jankowski, J. Jacobs, R. Kariots, and M. G. Lagally, J. Appl. Phys. **69**, 1411 (1991).
[5] J. B. Kortright, J. Appl. Phys. **70**, 3620 (1991).
[6] O. Renner, M. Kopecky, E. Krousky, F. Schufer, B. R. Muller, and N. I. Chkhalo, Rev. Sci. Instrum. **63**, 1478 (1992).
[7] J. B. Kortright and A. Fischer-Colbrie, J. Appl. Phys. **61**, 1130 (1987).
[8] S. K. Sinha, E. B. Sirota, S. Garoff, and H. B. Stanley, Phys. Rev. B **38**, 2297 (1988).
[9] V. Holy and T. Baumbach, Phys. Rev. B **49**, 10668 (1994).
[10] T. Salditt, T. H. Metzger, and J. Peisl, Phys. Rev. Lett. **73**, 2228 (1994).
[11] T. Salditt, D. Lott, T. H. Metzger, J. Peisl, G. Vignaud, J. F. Legrand, G. Grubel, P. Hoghoi, and O. Scharpf, Physica B **221**, 13 (1996).
[12] A. I. Volokhov, E. P. Kruglyakov, and N. I. Chkhalo, Surface **1**, 130 (1999). (in Russian).
[13] S. J. Sulyaev, N. V. Kovalenko, and V. A. Chernov, Surface **1**, 74 (2001) (in Russian).
[14] L. G. Parrat, Phys. Rev. **95**, 359 (1954).
[15] S. K. Sinha, M. K. Sanyal, S. K. Satija, C. F. Majkrzak, D. A. Neumann, H. Homma, S. Szpala, A. Gibaud, and H. Morkoç, Physica B **198**, 72 (1994).
[16] D. K. G. de Boer, Phys. Rev. B **53**, 6048 (1996).
[17] E. A. Kondrashkina, S. A. Stepanov, R. Opitz, M. Schimidbauer, R. Kohler, R. Hey, M. Wassermeier, and D. V. Novikov, Phys. Rev. B **56**, 10469 (1997).
[18] V. A. Chernov, E. D. Chkhalo, N. V. Kovalenko, and S. V. Mytnichenko, Nucl. Instrum. Methods Phys. Res. A **448**, 276 (2000).

Downloaded 15 May 2003 to 148.6.178.88. Redistribution subject to AIP license or copyright, see http://ojps.aip.org/japo/japcr.jsp